An oncolytic virus expressing a T cell engager simultaneously targets cancer and immunosuppressive stromal cells

Authors:

Joshua D. Freedman[1], Margaret R. Duffy[1], Janet Lei-Rossmann[1], Alice Muntzer[2], Eleanor M. Scott[1], Joachim Hagel[1,a], Leticia Campo[1], Richard J. Bryant[3], Clare Verrill[3,4], Adam Lambert[3], Paul Miller[5], Brian R. Champion[2], Leonard W. Seymour[1*], Kerry D. Fisher[1]

[1]*Department of Oncology, University of Oxford, UK.*

[2]*PsiOxus Therapeutics Ltd. Abingdon, UK*

[3]*Nuffield Department of Surgical Sciences, University of Oxford, Oxford, UK.*

[4]*Oxford NIHR Biomedical Research Centre, University of Oxford, Oxford, UK.*

[5]*Churchill Hospital, Oxford University Hospital NHS Trust, Oxford, UK.*

[a]*Current address: Experimental Medicine Division, Nuffield Department of Medicine, University of Oxford, UK*

[*]Corresponding author. Tel: +44 (0)1865 617020; Email: len.seymour@oncology.ox.ac.uk.

One Sentence Summary: Targeting T-cells to kill immune suppressive cancer associated fibroblasts using an oncolytic virus expressing a T-cell engager recognising fibroblast activation protein (FAP)

Running title: Oncolytic adenovirus expressing FAP BiTE

Statement of Significance (50 words): An engineered oncolytic adenovirus that encodes a bispecific antibody combines direct virolysis with endogenous T cell activation to attack stromal fibroblasts, providing a multimodal treatment strategy within a single therapeutic agent.

Conflict of interest: AM, BC, LWS and KDF own equity or share options in PsiOxus Therapeutics. The authors have no additional financial interests.

Abstract

Effective immunotherapy of stromal-rich tumors requires simultaneous targeting of cancer cells and immunosuppressive elements of the microenvironment. Here, we modified the oncolytic group B adenovirus enadenotucirev to express a stroma-targeted bispecific T cell engager (BiTE). This BiTE bound fibroblast activation protein on cancer-associated fibroblasts (CAF) and CD3ε on T cells, leading to potent T cell activation and fibroblast death. Treatment of fresh clinical biopsies, including malignant ascites and solid prostate cancer tissue, with FAP-BiTE-encoding virus induced activation of tumor-infiltrating PD1+ T cells to kill CAFs. In ascites, this led to depletion of CAF-associated immunosuppressive factors, upregulation of pro-inflammatory cytokines, and increased gene expression of markers of antigen presentation, T cell function, and trafficking. M2-like ascites macrophages exhibited a pro-inflammatory repolarisation, indicating spectrum-wide alteration of the tumor microenvironment. With this approach, we have actively killed both cancer cells and tumor fibroblasts, reversing CAF-mediated immunosuppression and yielding a potent single-agent therapeutic that is ready for clinical assessment.

Keywords: Oncolytic virus, adenovirus, FAP, BiTE, fibroblast

Introduction

Cancer-associated fibroblasts (CAFs) facilitate invasion (1), coordinate angiogenesis (2) and maintain an immune suppressive microenvironment in solid carcinomas (3). Their immunomodulatory functions include production of indoleamine 2,3-dioxygenase (IDO) and regulatory cytokines such as VEGF, FGF, IL-10 and TGFβ (4–8). Notably secreted TGFβ can accumulate in the stromal matrix, exerting a powerful immunosuppressive effect on newly-infiltrating naive immune cells (9,10), while CAF-produced CXCL12 can block entry of $CD8^+$ cells into the tumour and attract regulatory T-cells, inhibiting effector T-cell proliferation (11,12).

CAFs are pivotal to tumour immunology, making it difficult to envisage cancer immunotherapy achieving its full potential without addressing their deleterious effects. CAF depletion can reverse local immune suppression and improve tumour immunotherapy. Genetic-based CAF depletion in an autochthonous pancreatic cancer model uncovered the ability of anti-PDL1 to inhibit tumour growth and improve survival (13). Whilst such an approach has a strong therapeutic rationale, implementation can be difficult due to the lack of unique target antigens on the CAF surface, with most of their known surface markers also present on normal fibroblasts.

One promising target antigen is Fibroblast Activation Protein (FAP), which is upregulated on CAFs across a broad range of solid malignancies (14) but also found on normal fibroblasts in connective tissue in the muscle, gall bladder, bladder and bone marrow stromal cells (BMSCs) (15). Elimination of FAP-positive cells with monoclonal antibodies or FAP-targeted CAR-T-cells demonstrated the potential to reverse tumour-associated immune-suppression,

particularly when combined with immunotherapeutic strategies such as cancer vaccines (16,17). However, FAP expression on extra-tumoural cells is concerning, with previous FAP-targeting preclinical studies showing extensive bone marrow toxicity and cachexia that would caution against clinical development of systemic FAP-targeted treatments (15,18).

Bi-specific T-cell engagers (BiTE) show powerful targeted killing of cancer cells but can also be deployed against stromal targets such as CAFs. BiTEs crosslink T-cells (via CD3ε) to antigen-positive target cells, independent of HLA presentation, and can activate any T-cell to engage with and destroy adjacent target cells (19). Moreover, BiTE-mediated T-cell activation can overcome elements of tumour-associated immunosuppression that limit physiological immune responses, leading to re-activation and proliferation of exhausted tumour-specific T-cells (20–22). BiTEs targeted to a CAF marker such as FAP could be a potent strategy to activate intratumoural T-cells to attack and deplete CAFs. However, systemic delivery of the BiTE would likely mediate significant toxicity by activating circulating T-cells to attack normal fibroblasts and BMSCs. Accordingly, this potentially powerful approach is frustrated by challenges of site-specific delivery.

With their ability to encode and specifically express biologics in disseminated tumours, oncolytic viruses (OVs) are an ideal solution. One promising candidate is enadenotucirev (EnAd), which has demonstrated good blood-stability and systemic bioavailability in several early phase clinical trials (23–25). An encoded FAP-specific BiTE would be produced and secreted only upon virus infection of tumour cells, allowing it to access tumour-infiltrating lymphocytes (TILs). This approach has been validated using BiTEs to target T-cell cytotoxicity to tumour cell antigens (21,26–28). However, a virus-encoded BiTE that activates T-cells to

kill tumour stromal fibroblasts would provide a 'multimodal' therapeutic agent that simultaneously targets two distinct cell types within the tumour. Alongside direct OV-mediated cytolysis of tumour cells, which is often proinflammatory (29), secretion of FAP-specific BiTEs should activate TILs to attack and deplete CAFs, acting to reverse CAF-induced immune suppression. This approach combines direct cytotoxicity, immune-stimulation and reversal of local immune-suppression, thereby transforming an immunologically inactive 'cold' tumour into one that is 'hot', that is, with greater immune infiltration, yielding an integrated and more effective immunotherapeutic response.

Materials and Methods

Cell lines

DLD, SKOV3, A549, HEK293A (ATCC, USA) and NHDF (Lonza, Switzerland) cells were cultured in DMEM (Sigma-Aldrich, UK). Chinese Hamster Ovary (CHO, ATCC, USA), NHBE cells (Lonza, Switzerland) were cultured in RPMI-1640 (Sigma-Aldrich, UK). All cells were authenticated by STR profiling (CRUK Cambridge Institute, UK) and routinely tested each month for mycoplasma (MycoAlert Mycoplasma Detection Kit, Lonza). Cell lines were passaged no more than ten passages after thawing before use in experiments. Growth medium was supplemented with 10% (v/v) fetal bovine serum (FBS, Thermo Fisher, UK). Cells were incubated at 37°C and 5% CO_2. A FAP-expressing stable CHO cell line was generated using the FAP gene sequence (ID: 1149, NCBI) as previously described (21).

BiTE engineering and production

A FAP-targeted BiTE was produced by joining the DNA encoding two single-chain antibody fragments (scFvs) recognising human FAP and CD3ε with a sequence encoding a flexible glycine-serine (GS) linker. An N-terminal immunoglobulin signal sequence for mammalian secretion and C-terminal decahistidine tag for detection were added. DNA sequences were synthesised and inserted into a CMV promoter-driven expression vector (pSF-CMV-Amp; Oxford Genetics, UK) by standard cloning techniques. Recombinant BiTE protein was produced by transfecting HEK293A cells with polyethylenimine *(*PEI, linear, MW 25000, Polysciences, USA) (DNA:PEI ratio of 1:2 (w/w)). Cells maintained in serum-free DMEM. Supernatants were harvested, concentrated 50-fold using 10,000 MWCO Amicon Ultra-15 Filter Units (Millipore, UK), and stored at -80°C. BiTE protein concentration was determined by dot blot using decahistidine-tagged cathepsin D (Biolegend, UK) as a standard. Specific binding of the FAP BiTE to recombinant FAP protein was confirmed by ELISA (data not shown).

Generation of BiTE-expressing EnAdenotucirev

Modified EnAds were produced by direct insertion of the BiTE cassette into the parental EnAd cloning plasmid pEnAd2.4 using Gibson assembly (30,31). Additional viruses with FAP BiTE expression linked to RFP via a P2A site were also generated. Plasmid DNA was linearised by restriction digest with AscI (New England Biolabs, USA) and transfected into HEK293A cells for virus production in DMEM (2% FBS). Upon extensive plaque formation, cells were harvested, and virus released by three freeze-thaw cycles. Single clones were selected by serial dilution and amplified by serial infection, followed by double CsCl banding to produce concentrated virus stocks. Stocks were titred by the Quant-iT Picogreen dsDNA assay (Thermo Scientific, UK) and infectious dose determined by serial titration on A549 cells.

Processing and culture of human PBMCs and clinical biopsy samples

PBMCs were isolated from leukocyte cones (NHS Blood and Transplant, UK) by density gradient centrifugation. $CD3^+$ cells were extracted by depleting non-CD3 cells using the Pan T-cell Isolation Kit (Miltenyi Biotec, Germany). For $CD4^+$ and $CD8^+$ cells, $CD4^+$ Microbeads were used (Miltenyi Biotec). Primary human malignant ascites samples and human prostate tissue samples were obtained from the Churchill Hospital (Oxford University Hospitals NHS Foundation Trust) following written informed patient consent and approval by the institutional review board and research ethics committee of the Oxford Centre for Histopathology Research (Reference 09/H0606/5+5) in accordance to the UK Human Tissue Act 2004 and the Declaration of Helsinki. For ascites, samples were immediately processed with cells and fluid separated by centrifugation (300 g), with the cellular fractions treated with red blood cell lysis buffer (Qiagen, UK). For *ex vivo* T-cell activation and cytotoxicity, cells were used immediately, or adherent cells were expanded by serial passage. For human prostate tissue specimens, tissue was transported in RPMI and stored on ice until slicing within two hours of surgery. Tissue cores were embedded in UltraPure low melting-point agarose (4% w/v, Thermo Fisher, UK), and 300 μm tissue slices were prepared using a vibratome (Leica VT 1200S, Leica Microsystems, Germany). Each *ex vivo* tissue slice was transferred to a 0.6 cm^2 PTFE insert (Millipore, UK) in 24-well plates containing 1 mL of cultivation media for prostate tissue (Supplementary Material). After overnight culture, the media was replaced, and tissue slices were treated with BiTE or recombinant virus. On day zero, four and seven post-infection, 30% of the supernatant was collected, frozen and replaced. On day seven, slices were fixed in paraformaldehyde (4%) and embedded in paraffin for immunohistochemistry.

In vitro and *ex vivo* coculture experiments

For *in vitro* co-culture studies, PBMC were seeded with the appropriate target cells (E:T ratio,5:1) in flat bottom 96-well plates in 100 μL medium. Target cell lines were prepared with cell-dissociation buffer to preserve cell surface antigens. For *ex vivo* experiments, unpurified total cells from bone marrow or ascites were seeded in culture medium or fluid from the same exudate sample, respectively. To assess T-cell activation by virus-infected cells or BiTE-containing supernatants (300 ng/mL), co-cultures were treated with 100 μL supernatant or infected with 100 vp/cell in 100 μL medium. Where appropriate, CD3/CD28 Dynabeads (Thermo Fisher, UK) were included as positive controls for T-cell activation. T-cells were harvested by pooling the culture media and a subsequent PBS wash. If adherent cells are also required, cell-dissociation buffer was used to detach from plate surface and cells were pooled with non-adherent cells.

Characterisation of human T-cell activation

T-cell activation was measured by staining for surface expression of activation markers (CD69, CD25) and analysed by flow cytometry. To study T-cell proliferation, T-cells were labelled with 5 μM CFSE dye (Thermo Fisher, UK) prior to culturing with target cells. After five days, T-cells were harvested and analysed by flow cytometry. As a surrogate for proliferation in mixed cell populations (e.g. whole ascites samples), total T-cell number per well was determined using precision counting beads (Biolegend, UK). To measure T-cell degranulation, the externalisation of CD107a was assessed by adding a CD107a antibody directly to the well at the start of the experiment. After one-hour incubation, GolgiStop (6 μg/mL, BD Biosciences, USA) was added, followed by flow cytometry analysis after an additional five hours. IL-2 and IFNγ quantities were measured using the Human IL-2 ELISA MAX kit (Biolegend, UK) or

Human IFNγ ELISA MAX kit (Biolegend, UK). A flow cytometric multiplex bead immunoassay was performed using LEGENDplex Th Kit (Biolegend, UK).

Target cell cytotoxicity assay

To assess target cell cytotoxicity by free BiTE or virus, release of LDH into the supernatant (CytoTox 96 Non-Radioactive Cytotoxicity Assay, Promega, USA) or MTS viability assay (CellTiter 96 Cell Proliferation Assay, Promega, USA) were used. To determine viability of specific cell types, total cells were harvested by cell-dissociation buffer, and residual number of viable target cells measured by flow cytometry using an amine-reactive fluorescence live-dead stain. For observation of cell viability in real-time, xCELLigence technology (Acea Biosciences, USA) was used. TGFβ and VEGF quantities were measured using TGF beta-1 Human/Mouse ELISA Kit (Thermo Fisher, UK) and LEGENDplex Growth Factor Kit (Biolegend, UK), respectively.

Flow Cytometry

To classify different cellular populations, antibodies specific for CD11b (ICRF44), EpCAM (9C4), FAP (427819, R&D Systems, USA), CD3 (HIT3a), CD4 (OKT4), CD8a (HIT8) were used. To analyse T-cell populations, the following antigens were used: CD69 (FN50), CD25 (BC96), IFNγ (4S.B3), CD107a (H4A3), PD1 (H4A3). To analyse macrophage populations, cells were treated with Fc receptor block (Miltenyi Biotec, Germany) and stained with CD163 (GHI/61), CD206 (15-2), CD64 (10.1) and CD86 (IT2.2). The appropriate isotype control antibody was used in each case. All antibodies were acquired from Biolegend (UK) unless stated otherwise. Analysis was performed on a FACSCalibur flow cytometer (BD Biosciences, USA) and data processed with FlowJo v10.0.7r2 software (TreeStar Inc., USA).

Immunohistochemistry

Automated staining was carried out with the Leica BOND-MAX autostainer (Leica Microsystems, Germany). Antigen retrieval was performed at 100ºC using Epitope Retrieval Solution 2 (Leica Biosystems, Germany), followed by incubation with antibodies for CD8 (Agilent Technologies, USA), CD25 (Atlas Antibodies, Sweden), EpCAM (Biolegend, UK), FAP (R&D Systems, USA) or adenoviral hexon (Millipore, UK). Detection was performed using the BOND™ Polymer Refine Detection System (Leica Biosystems, Germany). Alternatively, for the FAP primary antibody only, anti-Sheep HRP-DAB Staining Kit (R&D Systems, USA) was used. Sections were incubated with haematoxylin and imaged (Aperio CS2 slice scanner (Leica Microsystems, Germany)).

Quantitative PCR (qPCR)

Adenovirus genomes were measured by qPCR using primers and probe against the hexon (primers: 5'-TACATGCACATCGCCGGA-3'/5'-C GGGCGAACTGCACCA-3', probe: 5'-FAM-CCGGACTCAGGTACTCCGAAGCATCCT-TAMRA-3'). At the specific timepoint, total cell and supernatants were harvested, and DNA extracted (PureLink Genomic DNA mini kit, Thermo Fisher, UK). In brief, primers and probe were mixed with DNA samples and added to QPCRBIO Probe Mix Hi-Rox (PCR Biosystems, UK) master mix. To measure levels of FAP mRNA in ascites, reverse-transcription qPCR was performed. The total cell fraction was harvested after 72 hours of treatment, RNA was extracted (RNAqueous™-Micro Total RNA Isolation Kit, Thermo Fisher, UK), and cDNA prepared (Superscript III First-Strand Synthesis SuperMix, Thermo Fisher, UK). FAP expression was quantified using FAP-specific primers (5'-TCAGTGTGAGTG CTCTCATTGTAT-3'/5'-GCTGTGCTTGCCTTATTGGT-3') and

2xqPCRBIO SyGreen Blue Mix Hi-ROX Master Mix (PCR Biosystems, UK). Expression of the 18S gene was also measured as a normalisation control (5'-GCCCGAAGCGTTTACTTTGA-3'/5'-TCCATTAT TCCTAGCTGCGGTATC-3'). All qPCR was run on ABI PRISM 7000 (Applied Biosystems, USA).

Gene expression analysis

Gene expression analysis was performed using the nCounter® PanCancer Immune Profiling Panel (NanoString Technologies, USA). The nSolver Advanced Analysis module was used for data analysis, in accordance with Nanostring® guidelines. Background thresholding was performed, followed by normalisation of the data via the mean of the internal NanoString positive controls, and differential expression determined, with reference to uninfected cells. A gene set's directed global significance score for a covariate measures the cumulative evidence for the up- or down-regulation of genes in a pathway and is calculated as the square root of the mean squared t-statistic of genes, with t-statistics generated from the linear regression algorithm within the nSolver Advanced Analysis module.

Microscopy

Brightfield and fluorescence images were obtained on a Zeiss Axiovert 25 microscope and captured with a Nikon DS5M camera. For time-lapse sequences, images were obtained on a Nikon TE 2000-E Eclipse inverted microscope and captured with a Hamamatsu Orca-ER C4742-95 using MetaMorph imaging software. Images were collected at 15 minutes intervals with videos (12 frames/second) generated using ImageJ software (NIH, USA). Where appropriate, cells were stained with CellTracker Orange CMTMR Dye (Thermo Fisher, USA)

and CellTrace Violet cell Proliferation Kit (Thermo Fisher, UK). Apoptosis was visualised using CellEvent Caspase 3/7 detection reagent (Thermo Fisher, UK).

Statistics

Where experiments produced two datasets, significance was evaluated using a student's two-tailed t-test. In all cases of more than two experimental conditions, statistical analysis was performed using a one-way ANOVA test with Tukey's *post hoc* analysis or two-way ANOVA test using Bonferroni *post hoc* analysis. All data is presented as mean ± standard deviation. Significance levels used were p = 0.01-0.05 (*), 0.001-0.01 (**), 0.0001-0.001 (***). Experiments were performed in biological triplicate, unless stated otherwise.

Results

Fibroblast-targeted BiTE engineering

A FAP-targeted BiTE was engineered recognising human FAP and CD3ε. A BiTE specific for CD3ε and an irrelevant antigen, filamentous haemagglutinin adhesin (FHA) of *Bordetella pertussis*, was used to control for unspecific binding. An N-terminal immunoglobulin signal sequence and C-terminal decahistidine tag were added for mammalian secretion and detection. BiTE protein production was assessed by transfection of HEK293A cells.

To confirm specificity of the FAP-BiTE for surface FAP, we established a human FAP-positive stable cell line using FAP-negative CHO cells. Peripheral blood mononuclear cell (PBMC)-derived T-cells were activated 24 h after co-culturing with CHO-FAP cells and FAP BiTE-

containing supernatants from transfected HEK293A (Fig. 1A) and mediated CHO-FAP cell lysis (Fig. 1B). Neither T-cell activation nor lysis were observed in cultures with parental CHO cells or control-BiTE, indicating that surface FAP expression is required for T-cell activation, presumably via surface CD3 clustering and pseudo-immunological synapse formation.

FAP-BiTE-to induce T-cell activation was also evaluated in co-culture with normal human dermal fibroblasts (NHDFs), which express surface FAP when cultured in high serum (10% FBS, Fig. S1A). Incubation of NHDF and PBMC-derived T-cells from six donors with FAP-BiTE-containing supernatants for 24 hours induced significant T-cell activation and NHDF lysis, with the control-BiTE having no effect (Fig. 1C; EC_{50}, 2.5 ng/mL). CFSE-labelled PBMC T-cells co-cultured with NHDF and FAP-BiTE underwent multiple rounds of T-cell proliferation (Fig. 1D) and showed at least 10-fold increase in IFNγ, IL-2, TNFα, IL-17F, IL-22 and IL-10 (Fig. 1E), with IFNγ production 10-fold higher than that induced by physiological anti-CD3/CD28 activation beads (Fig. 1F). Interestingly, FAP-BiTE induced activation and degranulation of CD4 and CD8 T-cells, directing both subsets to kill NHDF cells with similar potency (Fig. 1G-I). Importantly, no induction of activation markers, proliferation and cytokines was observed with control-BiTE or in the absence of NHDF target cells, confirming that CD3 clustering is essential for T-cell activation.

Generation of BiTE-armed enadenotucirev

Enadenotucirev (EnAd) is a conditionally-replicating chimeric group B adenovirus generated by bioselection (Fig. 2A)(32). The FAP-BiTE and control-BiTE sequences were inserted downstream of the fibre gene under transcriptional control of either an exogenous CMV promoter or a splice acceptor (SA) site for the adenoviral major late promoter (MLP). The

311 former drives immediate transgene expression upon successful cell infection, whereas MLP-
312 driven expression occurs only in cells permissive to virus replication, such as human tumour
313 cells. Viruses were rescued and purified from HEK293A cells (Table S1).

314

315 Colorectal adenocarcinoma (DLD) cells were infected at 100 vp/cell of the parental or
316 recombinant viruses to assess replication kinetics. Viral genome copies reached between 3-6 x
317 10^{12} genomes/ml (Fig. 2B), indicating that BiTE expression did not impair replication relative
318 to the parental virus. Cytotoxicity of all recombinant viruses was also comparable to parental
319 EnAd (Fig. 2C). Therefore, modification of the viral genome to incorporate the BiTE transgene
320 had little effect on viral replication or oncolytic activity.

321

322 FAP-BiTE secretion by virus-infected HEK293A cells was demonstrated by immunoblotting
323 of the supernatant (Fig. S1B). Functionality of these secreted virus-encoded BiTEs was
324 assessed by adding supernatants to co-cultures of PBMC-derived $CD3^+$ T-cells and either CHO
325 or CHO-FAP cells. T-cells co-cultured with CHO-FAP cells showed strong CD25 induction
326 and target cell lysis when incubated with supernatants from EnAd-CMV-FAPBiTE or EnAd-
327 SA-FAPBiTE-infected cells (Fig. 2D and 2E). No activation or cytotoxicity was observed with
328 supernatants from cells infected with unmodified or control-BiTE-expressing EnAd, in the
329 presence of parental CHO cells, or in the absence of T-cells. FAP-BiTE yield from DLD cells
330 infected with modified viruses was measured by comparing T-cell-mediated NHDF
331 cytotoxicity induced by 72-hour infected DLD supernatants to a standard curve. Following a
332 24-hour cytotoxicity assay, we measured FAP-BiTE at 9.8 and 49.2 $\mu g/10^6$ cells after 72 hours
333 for EnAd-CMV-FAPBiTE and EnAd-SA-FAPBiTE, respectively. This was consistent with
334 previous reports, suggesting that whilst transcriptional initiation is delayed, there is superior

total transgene expression when driven by the endogenous MLP compared to the CMV promoter (30). The FAP-BiTE showed impressive potency, with cytotoxicity detectable in supernatants diluted 10,000-fold (Fig. S1C).

EnAd-FAPBiTE-mediated oncolysis induces T-cell-mediated fibroblasts killing

EnAd kills carcinoma cell lines by direct oncolysis (33), but does not effectively replicate in, or directly kill, fibroblasts or other non-epithelial stromal cells (23). However, FAP-targeted BiTE from infected tumour cells should allow T-cell activation and mediate targeted killing of FAP-expressing stromal fibroblasts. Co-cultures of fibroblasts, moderately-permissive SKOV3 ovarian carcinoma cells (acting as BiTE producers) and T-cells, using moderately-permissive SKOV3 ovarian carcinoma cells which are killed by EnAd 5-7 days post-infection, and PBMC-derived T-cells were measured in real-time by cell index, a unitless measure of cell viability (Fig. 2F). In the absence of T-cells, tumour cells and fibroblasts cells persisted for 100-120 hours, independent of virus infection. In the presence of T-cells, FAP-BiTE expression from infected SKOV3 cells led to complete NHDF cytotoxicity, with lysis observed within 22 hours post-infection (hpi) by EnAd-CMV-FAPBiTE and 42 hpi for EnAd-SA-FAPBiTE. Crucially, no cytotoxicity was observed in cultures infected with EnAd or EnAd expressing the control-BiTE.

NHDF lysis was confirmed by lactate dehydrogenase (LDH) release in similar co-culture experiments (Fig. S1D). The kinetics of T-cell activation paralleled that of NHDF cytotoxicity (Fig. 2G and S1E). Importantly, FAP-BiTE-encoded viruses failed to induce CD25 expression

in the absence of NHDF, further demonstrating the requirement of FAP^+ cells for BiTE-mediated T-cell activation (Fig. S1F).

BiTE-induced cytotoxicity of stromal fibroblasts by T-cells was observed by time-lapse microscopy using co-cultures of T-cells, fibroblasts and DLD cells, which are more susceptible than SKOV3 cells to EnAd-mediated lysis (Fig. 2H, Movie S1-3). Whilst infection with EnAd induced dramatic DLD killing within 48 hours, NHDFs remained viable throughout. In contrast, EnAd-CMV-FAPBiTE infection induced both direct DLD killing and T-cell-mediated fibroblast cytotoxicity. Quantification of DLD and NHDF cells in parallel cultures showed complete elimination of both cell types upon treatment with EnAd-CMV-FAPBiTE or EnAd-SA-FAPBiTE 72 hpi (Fig. S1G).

EnAd-SA-FAPBiTE-mediated T-cell activation and target cell lysis is tumour-selective

Conventional FAP-targeted therapeutics given intravenously are reported to induce FAP^+ cell toxicity within the bone marrow compartment (18). Coupling BiTE expression to virus replication via the viral MLP restricts expression to the tumour compartment, minimising unwanted toxicity to FAP^+ fibroblasts in normal physiological sites. To compare selectivity of virally encoded CMV- and MLP-driven BiTE expression, NHDFs were incubated with EnAd, EnAd-CMV-FAPBiTE or EnAd-SA-FAPBiTE in the presence of primary T-cells only. At 72 hpi with EnAd-CMV-FAPBiTE, we observed cytotoxicity in 80% of NHDF cells (Fig. 3A). No lysis was observed in EnAd-SA-FAPBiTE-infected cells, consistent with the inability of EnAd to complete its life cycle in non-epithelial tumour cells (23).

To better simulate the multiple cell types present in a healthy tissue, NHDFs were cultured with exogenous PBMC-derived T-cells and either normal human bronchial epithelial (NHBE) cells or SKOV3 and subsequently infected with EnAd-SA-FAPBiTE or EnAd-SA-controlBiTE. While EnAd-SA-FAPBiTE infection of SKOV3 allowed T-cell activation and target cell lysis (Fig. 3B-D), NHBE cells did not.

Finally, for maximum clinical relevance, EnAd-SA-FAPBiTE activity was evaluated in three fresh human whole bone marrow samples from healthy donors. Despite literature reports of bone marrow toxicity of FAP-targeted antibodies, no FAP^+ cells were detected in any samples. Accordingly FAP^+ NHDF 'target' cells were added prior to infection to determine whether our armed viruses triggered uncontrolled toxicity against FAP^+ cells. Neither EnAd-SA-FAPBiTE nor EnAd-SA-controlBiTE induced endogenous T-cell activation in the absence of tumour cells (Fig. 3E) or cytotoxicity (Fig. 3F). The addition of SKOV3 cells led to T-cell activation and cytotoxicity following EnAd-SA-FAPBiTE infection, with the latter thought to reflect predominantly BiTE-mediated T cell lysis of FAP^+ NHDFs. These data confirm that MLP-driven FAP-BiTE production is restricted to tumour cells and suggest there should be no systemic toxicity against FAP^+ cells within normal bone marrow.

EnAd expressing FAP-BiTE activates tumour-associated T-cells to kill endogenous fibroblasts within patient-derived malignant ascites

Malignant peritoneal ascites are frequent in several advanced carcinoma types, including ovarian, pancreatic, breast and lung cancers (34), and often associated with a poor prognosis (34,35). The fluid is routinely drained from some patients as a palliative treatment, providing a convenient and informative liquid biopsy. There is mounting evidence that malignant ascites

405 are sites of substantial immune-suppression (36). We therefore assessed the effects of cell-free
406 ascites fluid on PBMC-derived T-cell activation using anti-CD3/CD28 beads and FAP-BiTE.
407 Bead-mediated T-cell activation was significantly inhibited by 3/5 ascites samples (Fig. 4A).
408 In contrast, FAP-BiTE-mediated T-cell activation was not suppressed by any ascites fluids
409 compared to levels observed in normal serum (Fig. 4B).

410

411 Human ascites biopsy samples typically contain tumour cells, fibroblasts, lymphocytes and
412 macrophages, representing a unique tumour-like model system to assess endogenous tumour-
413 associated T-cell activation. Figure 4C shows the cellular composition of a representative
414 sample containing $CD3^+$, $EpCAM^+$, $CD11b^+$ and FAP^+ cells (see also Fig. S2A-B and Table
415 S2). Ascites-associated $CD3^+$ T-cells were, on average, 63% (up to 92.5%) positive for the
416 exhaustion marker PD1 compared to only 10-20% of PBMC-derived T-cells (Fig. 4D). We
417 assessed the ability of BiTE-encoding EnAd to infect ascites cancer cells and secrete sufficient
418 amounts of BiTE, leading to endogenous T-cell activation and killing of autologous cancer-
419 associated fibroblasts within an ascites sample. Total ascites cells from four patient biopsies
420 were incubated in 50% ascites fluid with free FAP-BiTE or EnAd encoding FAP-BiTE. After
421 five days, endogenous T-cells were strongly activated in all ascites biopsy samples (30-80% of
422 total $CD3^+$ cells, Fig. 4E), combined with $CD3^+$ T-cell proliferation (Fig. 4F). Parental and
423 control-BiTE viruses did not induce T-cell activation or proliferation.

424

425 Ascites T-cell activation and cytotoxicity towards endogenous FAP^+ fibroblasts was assessed
426 by measuring the change in FAP^+ cell number during treatment (Fig. 4G). Free FAP-BiTE and
427 EnAd-CMV-FAPBiTE induced significant depletion of FAP^+ fibroblasts in all samples,
428 typically to levels below 1% of those in untreated or control samples, consistent with marked

falls in FAP mRNA, VEGF secretion, and elimination of cells with a fibroblast-like morphology (Fig. S3A-C). A similar trend was observed upon infection with EnAd-SA-FAPBiTE, although one patient (patient biopsy 1) demonstrated neither T-cell activation nor fibroblast depletion (Fig. 4E and 4G). Infection of this sample with EnAd-SA-GFP also showed no GFP-positive cells (Fig. S3D, Table S2) and no $EpCAM^+$ tumour cells at the outset (Fig. S3E). The sample likely had insufficient tumour cells to support virus replication, demonstrating the strict necessity of tumour cells for virus replication and MLP-drive BiTE expression, suggesting one predictor for potency. A cytokine array of patient biopsy 1 demonstrated that EnAd-CMV-FAPBiTE infection induced at least 10-fold increases in IL-17A, IL-17F, IL-22, IFNγ and IL-10 expression (Fig. 4H). Parallel experiments using expanded mixed cultures of ascites-derived fibroblasts and tumour cells showed that fibroblast depletion led to 50-70% lower TGFβ levels in supernatants (Fig. 4I), suggesting FAP^+ cells to be a major source of immune-suppressive TGFβ within tumour ascites. Altogether, these data show that treatment of malignant ascites with free or virally-encoded FAP-BiTE is able to polyclonally activate anergic T-cells, leading to targeted depletion of autologous tumour-associated fibroblasts.

Global changes in immune pathway gene expression were observed in EnAd-SA-FAP-BiTE-treated samples

To assess the impact of CAF depletion, T-cell activation and virolysis of cancer cells on the tumour microenvironment, we used Nanostring to determine changes in the expression of 730 cancer and immune pathway genes in three primary ascites samples, selected to represent the spectrum of clinical possibilities. Biopsy 4 had a high ratio of FAP^+ cells relative to $EpCAM^+$

cells (likely epithelial cancer cells; Table S3), while biopsy 5 had a similar proportion of $EpCAM^+$ and FAP^+ cells, and biopsy 6, a relatively low ratio of FAP^+ to $EpCAM^+$ cells. All samples had similar levels of $CD3^+$ T-cells and $CD11b^+$ myeloid cells.

Significant T-cell activation was observed in all samples three days post-infection with EnAd-SA-FAPBiTE, but not EnAd-SA-controlBiTE (Fig. S4A). Approximately 40% of all genes showing significant changes in mRNA levels of at least two-fold (Fig. S4B); only mRNA basally expressed above a minimum threshold level were included in the analysis. Considerably more genes showed changes following exposure to EnAd-SA-FAPBiTE than EnAd-SA-controlBiTE, except biopsy 6, where the high number of $EpCAM^+$ cancer cells may have resulted in extensive EnAd-specific gene changes due to BiTE-independent direct virolysis. Changes were grouped by immune response category as an average of three samples (Fig. 5A) or individual samples (Fig. S4C). Although individual biopsies showed some variation, all EnAd-SA-FAPBiTE-infected samples demonstrated increased gene expression in numerous immune groupings including cytotoxicity, pathogen defence and T-cell, B cell and NK cell function. Whilst T-cell- and NK cell-attractant chemokines (CXCL9, CXCL10, CXCL11) were also upregulated in all biopsies, strong decreases in fibroblast-associated CXCL6, CXCL12 and CXCL14 induced a downregulation in overall chemokine expression for biopsy 4 (Fig. S4D).

Figure 5B shows the data set for biopsy 4 which had the highest number of FAP^+ cells. The most highly upregulated genes (up to 100-fold) following treatment with EnAd-SA-FAPBiTE included T-cell markers (granzyme B, perforin, IFNγ, TNF, IL2RA/CD25). The greatest decreases (up to 1000-fold) were in fibroblast-associated genes, such as collagen type III,

fibronectin, thy-1, CXCL12 and IL-13Rα2. Similar trends were seen across all three samples, with the most modest changes in fibroblast markers observed in biopsy 6, which had the lowest levels of FAP^+ cells. Changes in expression of key genes compared to untreated samples are shown by individual biopsy in Fig. 5C-F. For example, expression of the fibroblast marker collagen type III (COL3A1) is dramatically reduced upon infection with EnAd-FAPBiTE compared to EnAd-controlBiTE in all three samples, while thy-1 and IL-13Rα2 (also used as fibroblast markers; Fig. 5C) showed FAP-BiTE-dependent decreases in two biopsies. Basal expression of these genes in biopsy 6 did not pass the minimum threshold for analysis. T-cell activation markers (granzyme B, perforin and IL2RA/CD25; Fig. 5D), checkpoint markers (PD1, CTLA4 and LAG3; Fig. S4E), T-cell recruiting chemokine CXCL9 and DC maturation/antigen presentation markers LAMP3 and TAP1 (Fig. 5E) all increased in a FAP-BiTE-dependent manner. These latter findings are particularly encouraging, raising the possibility of immunosuppression reversal in the tumour microenvironment following EnAd-SA-FAPBiTE infection.

Treatment of ascites samples with EnAd-SA-FAPBiTE induces repolarisation of resident tumour-associated macrophages

Macrophages are known to show plasticity between pro-inflammatory ‘M1’ and wound-healing ‘M2’ phenotypes, with tumour-associated macrophages (TAMs) usually skewed towards ‘M2’. To investigate the influence of FAP-BiTE on macrophage polarisation, patient-derived malignant ascites samples were treated with free or EnAd-encoded FAP-BiTE to determine activation of endogenous T-cells and $CD11b^+CD64^+$ cells. Treatment with free FAP-BiTE or EnAd-SA-FAPBiTE induced strong T-cell activation and IFNγ secretion (Fig. S4F).

We observed simultaneous induction of an activated M1-like macrophage phenotype, manifested by strong decreases in CD206 and CD163 (Fig. 5F) and increased CD64 expression (Fig. 5G). Infection with EnAd-SA-FAPBiTE induced a large increase in CD86 expression, while free FAP-BiTE, EnAd-SA-controlBiTE or IFNγ alone had no effect (Fig. 5G).

EnAd-SA-FAPBiTE activates TILs and induces BiTE-mediated cytotoxicity in solid prostate tumour biopsies

We obtained seven fresh paired punch biopsies of malignant prostate tissue from patients undergoing radical prostatectomy, cut into thin sections for *ex vivo* cultures. Prostate tissue slices showed a characteristically complex architecture, with glandular structures of (malignant) $EpCAM^+$ epithelial cells interspersed with large regions of intervening stroma containing scattered CD8 T-cells (Fig. S5A). FAP expression was generally weak in benign prostate tissue and high in malignant prostate tissue (Fig. 6A). Fibroblasts showing the strongest FAP expression were often adjacent to malignant epithelial cells (Fig. S5A).

To facilitate assessment of virus activity, we developed reporter viruses linking FAP-BiTE and red fluorescent protein (RFP) expression (Fig. S5B). Following infection with EnAd-SA-FAPBiTE-RFP, malignant tissue slices showed RFP expression, demonstrating successful viral infection, replication and BiTE expression (Fig. S5C). Positive staining for viral hexon confirmed EnAd replication, apparently limited to malignant epithelial cells (Fig. 6B). Malignant prostate tissue infected with EnAd-SA-FAPBiTE showed an increase in activated endogenous TILs seven days post-infection (Fig. 6C). Slices from all patients showed significant induction of IFNγ production, with IL-2 levels also increasing in four samples (Fig. 6D and 6E); both cytokines are associated with activated CD4 Th1 and CD8 cytotoxic T-cells

(37). Neither untreated slices nor those infected with EnAd-SA-controlBiTE-RFP showed detectable T-cell activation, though some samples demonstrated modest increases in IFNγ and IL-2 following EnAd-SA-controlBiTE-RFP infection, likely a direct result of virolysis. In benign prostate tissue, there was little increase in IFNγ or IL-2 with any treatment (Fig. S5D-E).

BiTE-mediated activation of T-cells is expected to lead to fibroblast killing. Cells were visualised undergoing apoptosis in real-time within *ex vivo* prostate tissues (Fig. 6F). EnAd-SA-FAPBiTE-RFP-infected cells strongly associated with apoptotic nuclei, suggesting BiTE-mediated induction of proximal cytotoxicity of surrounding cells. FAPBiTE-mediated cytotoxicity was observed in all patient biopsy samples, with intrinsic EnAd activity also inducing small increases, potentially due to a greater number of cancer cells in some samples (Fig. 6G). Indeed, regions of high T-cell activation showed an absence or degradation of surrounding tissue or stroma, with tissue architecture remaining intact in uninfected samples (Fig. 6H). Crucially, FAP^{low} benign prostate tissue showed negligible increases in cytotoxicity within the duration of the study (Fig. S5F).

Discussion

Here, we have developed an armed oncolytic adenovirus combining three distinct therapeutic strategies: direct virus-mediated cytotoxicity towards cancer cells, creation of a proinflammatory immune environment, and removal of a key stromal cell mediator of tumour immunosuppression. Encoding BiTEs within OVs exploits the strengths of both virotherapy

and immunotherapy whilst overcoming limitations of each agent alone. When expressed locally, the short plasma half-lives of BiTEs will become advantageous, minimising systemic exposure and avoiding "on-target, off-tumour" toxicities (38). Conversely, arming an OV with a BiTE provides an additional mechanism of cell killing and broadens the range of target cells to include OV-resistant stromal cells.

Combining OVs and BiTEs also has a potentially synergistic effect on infiltrating T-cells. Increased $CD8^+$ T-cell infiltration into the tumour bed has been observed in several OV clinical trials, including studies using EnAd and FDA-approved Imlygic (24,39), likely providing more effector cells for BiTE-mediated cytotoxicity. Simultaneously, BiTE-mediated redirection of TILs (potentially virus-specific) towards chosen targets may delay viral clearance and increase intratumoural spread.

For maximal translational relevance, our current and future studies will focus on primary human tumour biopsies maintained *ex vivo*, rather than compromise with imperfect murine models that may not provide the desired tumour heterogeneity or realistic levels of immune suppression (23,40). Clinical samples retain the heterogeneous and multifaceted cellular interactions of advanced human cancer, and, in the case of organotypic prostate tumour slices, the stromal architecture and extracellular matrix of a solid tumour. Treatment of both solid and liquid tumour biopsies with EnAd-FAP-BiTE led to tumour-associated T-cell activation and destruction of endogenous FAP^+ fibroblasts, alongside secretion of large quantities of pro-inflammatory cytokines and chemokines, including IFNγ, IL-2, TNFα, IL-17, and CXCL9. Crucially, this demonstrated that the patient's own tumour-associated T-cells can be used for therapeutic purposes in the realistic environment of an advanced human tumour. It was

particularly encouraging that T-cells within all tested patient biopsies, shown to be $PD1^+$ and likely anergic, were readily activated and rendered functional by the BiTE to mediate cytotoxicity. This may reflect the high level of activating stimuli each T-cell can receive using a BiTE, where in principle every CD3 can be crosslinked to the target antigen (>100,000 copies per cell) without being limited by the relatively small number of HLA-presented TCR-cognate peptides available, likely to be less than 100 per cell. Indeed, the efficacy of BiTE-mediated T-cell stimulation is augmented when targeting a high-density receptor like FAP, a result also seen with other antigens (21,22).

Nanostring analysis confirmed the extensive depletion of fibroblast-associated RNA in human malignant ascites samples treated with EnAd-FAPBiTE, together with strong induction of genes involved in T-cell function. Despite their varying cellular compositions, similar immune-activating trends were seen in all samples following EnAd-FAPBiTE infection, with stimulation of RNAs involved in leukocyte trafficking, dendritic cell maturation and antigen presentation. Surface markers on ascites TAMs revealed a clear shift from an M2-like phenotype to one that is more pro-inflammatory. We expect that newly-infiltrating monocytes, recruited by OV-mediated induction of monocyte-attractant chemokines, such as CCL2, CCL7 and RANTES, will acquire an M1 ‘activated’ phenotype. Significantly, surface expression of costimulatory ligand CD86 on TAMs was only induced by the combination of virus and FAP-BiTE (EnAd-FAPBiTE). We hypothesise that virus stimulation of pathogen-associated molecular patterns, interferon signalling, or STING and removal of CAF-mediated suppression are required for CD86 activation. These findings indicate that coupling CAF depletion with potent activatory stimuli (T-cell activation and viral-mediated immunogenic cell death) synergistically re-polarise the tumour microenvironment towards promotion of an effective anticancer immune response (41). Similarly, though we expect that suppressive markers will

increase in tandem with activation markers, this potential barrier to continued virus activity could be counteracted by combining OVs with checkpoint inhibitors.

Using OVs for cancer-targeted transgene expression has now been validated both pre-clinically and clinically (24,42). Here, we regulated BiTE expression using the adenoviral MLP, limiting BiTE production to cells permissive to the virus life cycle. In the absence of cancer cells, we observed no BiTE production or cytotoxicity (Fig. 3). This is particularly important in light of the "on-target off-tumour" toxicities observed with FAP-targeted antibodies or CAR-T-cells towards FAP^+ bone marrow cells. Infection of primary cultures of freshly isolated human bone marrow by EnAd-SA-FAPBiTE showed no T-cell activation or bone marrow cell toxicity in the absence of tumour cells. Endogenous FAP+ cells also likely occur at frequencies too low (~0.01%) to identify in the mononuclear cell fraction. Hence, our elegant targeted-expression strategy is expected to avoid such toxicities whilst exploiting the potent effects of the FAP-BiTE within the microenvironment of each tumour deposit.

We therefore believe that arming OVs to express BiTEs targeting stromal elements, such as CAFs, can provide a powerful new multimodal approach to cancer therapy. In this way, a single agent actively kills two different cell types using two distinct, yet targeted, cytotoxic mechanisms. EnAd provides a particularly promising virus platform to achieve targeted BiTE expression in disseminated tumours, exploiting the blood stability and systemic bioavailability of the virus, which has been studied in several early-phase clinical trials. This strategy to induce proinflammatory cell death whilst reversing TME-mediated immunosuppression may be what is ultimately required to turn intransigent, stromal-rich carcinomas into targets for a complete and durable immunotherapeutic response.

Acknowledgements

The authors gratefully acknowledge support from the Medical Research Council (MRC-Oxford Doctoral Training Partnership, MR/K501256/1, JD Freedman) and Cancer Research UK (Grant #C552/A17720, J Lei-Rossmann, K Fisher, L Seymour; Studentship C5255/A20936, EM Scott). MR Duffy is funded by the Kay Kendall Leukaemia Fund (grant KKL1050). J.Lei-Rossmann is supported by Linacre College, Oxford. pEnAd2.4 was kindly provided by PsiOxus Therapeutics. We are grateful to Egon Jacobus (University of Oxford) for the use of his primers. Special thanks to Alison Carr and her team for their helpful collection of ascites. C. Verrill's research time is part-funded by the Oxford NIHR Biomedical Research Centre (Molecular Diagnostics Theme/Multimodal Pathology Subtheme). We acknowledge the contribution to this study made by the Oxford Centre for Histopathology Research and the Oxford Radcliffe Biobank, which are supported by the NIHR Oxford Biomedical Research Centre.

Conflict of interest: AM, BC, LWS and KDF own equity or share options in PsiOxus Therapeutics. The authors have no additional financial interests.

References

1. Itoh G, Chida S, Yanagihara K, Yashiro M, Aiba N, Tanaka M. Cancer-associated fibroblasts induce cancer cell apoptosis that regulates invasion mode of tumours. Oncogene. 2017;36:4434–44.

2. Tang D, Gao J, Wang S, Ye N, Chong Y, Huang Y, et al. Cancer-associated fibroblasts promote angiogenesis in gastric cancer through galectin-1 expression. Tumor Biol. 2016;37:1889–99.

3. Harper J, Sainson RCAA. Regulation of the anti-tumour immune response by cancer-associated fibroblasts. Semin. Cancer Biol. 2014 page 69–77.

4. Connell JTO, Sugimoto H, Cooke VG, MacDonald BA, Mehta AI, LeBleu VS, et al. VEGF-A and Tenascin-C produced by S100A4+ Stromal Cells Are Important for Metastatic Colonization. Proc Natl Acad Sci. 2011;108:16002–7.

5. Henriksson ML, Edin S, Dahlin AM, Oldenborg P-AA, Öberg Å, Van Guelpen B, et al. Colorectal cancer cells activate adjacent fibroblasts resulting in FGF1/FGFR3 signaling and increased invasion. Am J Pathol. 2011;178:1387–94.

6. Kojima Y, Acar A, Eaton ENN, Mellody KT, Scheel C, Ben-Porath I, et al. Autocrine TGF- and stromal cell-derived factor-1 (SDF-1) signaling drives the evolution of tumor-promoting mammary stromal myofibroblasts. Proc Natl Acad Sci. 2010;107:20009–14.

7. Chen JY, Li CF, Kuo CC, Tsai KK, Hou MF, Hung WC. Cancer/stroma interplay via cyclooxygenase-2 and indoleamine 2,3-dioxygenase promotes breast cancer progression. Breast Cancer Res. 2014;16:410.

8. Soliman H, Mediavilla-Varela M, Antonia S. Indoleamine 2,3-dioxygenase: is it an

immune suppressor? Cancer J. 2010;16:354–9.

9. Taipale J, Saharinen J, Keski-Oja J. Extracellular matrix-associated transforming growth factor-beta: role in cancer cell growth and invasion. Adv Cancer Res. 1998;75:87–134.

10. Flavell RA, Sanjabi S, Wrzesinski SH, Licona-Limón P. The polarization of immune cells in the tumour environment by TGFbeta 2. Nat Rev Immunol. 2010;10:554–67.

11. Fearon DT. The Carcinoma-Associated Fibroblast Expressing Fibroblast Activation Protein and Escape from Immune Surveillance. Cancer Immunol Res. 2014;2:187–93.

12. Costa A, Kieffer Y, Scholer-Dahirel A, Pelon F, Bourachot B, Cardon M, et al. Fibroblast Heterogeneity and Immunosuppressive Environment in Human Breast Cancer. Cancer Cell. 2018;33:463–479.e10.

13. Feig C, Jones JO, Kraman M, Wells RJB, Deonarine A, Chan DS, et al. Targeting CXCL12 from FAP-expressing carcinoma-associated fibroblasts synergizes with anti-PD-L1 immunotherapy in pancreatic cancer. Proc Natl Acad Sci. 2013;110:20212–7.

14. Garin-Chesa P, Old LJ, Rettig WJ. Cell surface glycoprotein of reactive stromal fibroblasts as a potential antibody target in human epithelial cancers. Proc Natl Acad Sci. 1990;

15. Roberts EW, Deonarine A, Jones JO, Denton AE, Feig C, Lyons SK, et al. Depletion of stromal cells expressing fibroblast activation protein-α from skeletal muscle and bone marrow results in cachexia and anemia. J Exp Med. 2013;210:1137–51.

16. Wang L-CS, Lo A, Scholler J, Sun J, Majumdar RS, Kapoor V, et al. Targeting fibroblast activation protein in tumor stroma with chimeric antigen receptor T cells can inhibit tumor growth and augment host immunity without severe toxicity. Cancer Immunol Res.

2014;2:154–66.

17. Ostermann E, Garin-Chesa P, Heider KH, Kalat M, Lamche H, Puri C, et al. Effective immunoconjugate therapy in cancer models targeting a serine protease of tumor fibroblasts. Clin Cancer Res. 2008;14:4584–92.

18. Tran E, Chinnasamy D, Yu Z, Morgan RA, Lee C-CR, Restifo NP, et al. Immune targeting of fibroblast activation protein triggers recognition of multipotent bone marrow stromal cells and cachexia. J Exp Med. 2013;210:1125–35.

19. Brischwein K, Schlereth B, Guller B, Steiger C, Wolf A, Lutterbuese R, et al. MT110: A novel bispecific single-chain antibody construct with high efficacy in eradicating established tumors. Mol Immunol. 2006;43:1129–43.

20. Dao T, Pankov D, Scott A, Korontsvit T, Zakhaleva V, Xu Y, et al. Therapeutic bispecific T-cell engager antibody targeting the intracellular oncoprotein WT1. Nat Biotechnol. 2015;33:1079–86.

21. Freedman JD, Hagel J, Scott EM, Psallidas I, Gupta A, Spiers L, et al. Oncolytic adenovirus expressing bispecific antibody targets T-cell cytotoxicity in cancer biopsies. EMBO Mol Med. 2017;9:1067–87.

22. Deisting W, Raum T, Kufer P, Baeuerle PA, Münz M. Impact of diverse immune evasion mechanisms of cancer cells on T cells engaged by EpCAM/CD3-bispecific antibody construct AMG 110. Chatenoud L, editor. PLoS One. 2015;10:e0141669.

23. Illingworth S, Di Y, Bauzon M, Lei J, Duffy MR, Alvis S, et al. Preclinical Safety Studies of Enadenotucirev, a Chimeric Group B Human-Specific Oncolytic Adenovirus. Mol Ther - Oncolytics. 2017;5:62–74.

706 24. Garcia-Carbonero R, Salazar R, Duran I, Osman-Garcia I, Paz-Ares L, Bozada JM, et
707 al. Phase 1 study of intravenous administration of the chimeric adenovirus
708 enadenotucirev in patients undergoing primary tumor resection. J Immunother Cancer.
709 2017;5:71.

710 25. Calvo E, Martín MG, Cubillo A, Machiels J, Rottey S, Mardjuadi F, et al. 1064P A phase
711 1 study of enadenotucirev, an oncolytic Ad11/Ad3 chimeric group B adenovirus,
712 administered intravenously - analysis of dose expansion and repeat cycle cohorts in
713 patients with metastatic colorectal cancer (MCRC). Ann Oncol. Oxford University
714 Press; 2014;25:iv367-iv367.

715 26. Speck T, Heidbuechel JPWW, Veinalde RR, Jaeger D, von Kalle C, Ball CR, et al.
716 Targeted bite expression by an oncolytic vector augments therapeutic efficacy against
717 solid tumors. Clin Cancer Res. 2018;24:2128–37.

718 27. Fajardo CA, Guedan S, Rojas LA, Moreno R, Arias-Badia M, De Sostoa J, et al.
719 Oncolytic adenoviral delivery of an EGFR-targeting t-cell engager improves antitumor
720 efficacy. Cancer Res. 2017;77:2052–63.

721 28. Yu F, Wang X, Guo ZS, Bartlett DL, Gottschalk SM, Song X-TT. T-cell engager-armed
722 oncolytic vaccinia virus significantly enhances antitumor therapy. Mol Ther.
723 2014;22:102–11.

724 29. Guo ZS, Liu Z, Bartlett DL. Oncolytic Immunotherapy: Dying the Right Way is a Key
725 to Eliciting Potent Antitumor Immunity. Front Oncol. 2014;4:74.

726 30. Marino N, Illingworth S, Kodialbail P, Patel A, Calderon H, Lear R, et al. Development
727 of a versatile oncolytic virus platform for local intra-tumoural expression of therapeutic
728 transgenes. PLoS One. 2017;12:e0177810.

729 31. Gibson DG, Young L, Chuang R-YY, Venter JC, Hutchison CA, Smith HO. Enzymatic
730 assembly of DNA molecules up to several hundred kilobases. Nat Methods.
731 2009;6:343–5.

732 32. Kuhn I, Harden P, Bauzon M, Chartier C, Nye J, Thorne S, et al. Directed evolution
733 generates a novel oncolytic virus for the treatment of colon cancer. PLoS One [Internet].
734 2008 [cited 2016 Feb 9];3:e2409. Available from:
735 http://www.pubmedcentral.nih.gov/articlerender.fcgi?artid=2423470&tool=pmcentrez
736 &rendertype=abstract

737 33. Dyer A, Di Y, Calderon H, Illingworth S, Kueberuwa G, Tedcastle A, et al. Oncolytic
738 Group B Adenovirus Enadenotucirev Mediates Non-apoptotic Cell Death with
739 Membrane Disruption and Release of Inflammatory Mediators. Mol Ther - Oncolytics.
740 2017;4:18–30.

741 34. Ayantunde AA, Parsons SL. Pattern and prognostic factors in patients with malignant
742 ascites: A retrospective study. Ann Oncol. 2007;18:945–9.

743 35. Zamboni MM, da Silva CT, Baretta R, Cunha ET, Cardoso GP. Important prognostic
744 factors for survival in patients with malignant pleural effusion. BMC Pulm Med.
745 2015;15:29.

746 36. Simpson-Abelson MR, Loyall JL, Lehman HK, Barnas JL, Minderman H, O'Loughlin
747 KL, et al. Human ovarian tumor ascites fluids rapidly and reversibly inhibit T cell
748 receptor-induced NF-κB and NFAT signaling in tumor-associated T cells. Cancer
749 Immun. 2013;13:14.

750 37. Romagnani S. Lymphokine Production by Human T Cells in Disease States. Annu Rev
751 Immunol. 1994;12:227–57.

38. Teachey DT, Rheingold SR, Maude SL, Zugmaier G, Barrett DM, Seif AE, et al. Cytokine release syndrome after blinatumomab treatment related to abnormal macrophage activation and ameliorated with cytokine-directed therapy. Blood. 2013;121:5154–7.

39. Ribas A, Dummer R, Puzanov I, VanderWalde A, Andtbacka RHI, Michielin O, et al. Oncolytic Virotherapy Promotes Intratumoral T Cell Infiltration and Improves Anti-PD-1 Immunotherapy. Cell. 2017;170:1109–1119.e10.

40. Lei J, Jacobus EJ, Taverner WK, Fisher KD, Hemmi S, West K, et al. Expression of human CD46 and trans-complementation by murine adenovirus 1 fails to allow productive infection by a group B oncolytic adenovirus in murine cancer cells. J Immunother Cancer. 2018;6:55.

41. Weerasinghe P, Buja LM. Oncosis: An important non-apoptotic mode of cell death. Exp Mol Pathol. 2012;93:302–8.

42. Miller A, Russell SJ. The use of the NIS reporter gene for optimizing oncolytic virotherapy. Expert Opin Biol Ther. 2016;16:15–32.

Figure Legends

Fig. 1. FAP-BiTE-containing supernatants activate primary human T-cells and target cytotoxicity to FAP$^+$ cells. (A) Activation ($CD69^+CD25^+$) of primary human CD3 cells cultured for 24 hours with BiTE-containing supernatants and CHO or CHO-FAP cells. **(B)** LDH release by target cells in (A). **(C)** CD25 expression on T-cells (black) and NHDF lysis (LDH release, red), were assessed after 24 hours of co-culture with BiTE and PBMC-derived T-cells from six healthy donors. **(D)** Representative proliferation of CFSE-stained T-cells after five-day co-culture with BiTE and NHDFs. **(E)** Cytokine production was evaluated by a multiple human Th cytokine panel after co-culturing T-cells with BiTE and NHDFs for 48 hours. **(F)** Secreted IFNγ from co-cultures of T-cells with NHDF and BiTE-containing supernatants. **(G, H)** Induction of CD25 (G) or degranulation (H) of CD4 and CD8 T-cells following 24 hours co-culture with BiTE and NHDFs. **(I)** LDH release by NHDF cells after 24 hours in co-cultures with BiTE and either CD4- or CD8-purified T-cells.

(A-C,E-I) Data show mean ± SD of biological triplicates. Significance was assessed using one-way ANOVA with Tukey's Post Hoc analysis compared to 'untreated' (A, C, E, F) or 'control-BiTE' (B) or using an unpaired two-tailed t-test (G-I); *, $p<0.05$; **, $p<0.01$; ***, $p<0.001$.

Fig. 2. EnAd expressing FAP-BiTE induces T-cell-dependent cytotoxicity of stromal fibroblasts. (A) Genome of the BiTE-armed oncolytic adenovirus, enadenotucirev (EnAd). ITR, inverted terminal repeat; P, promoter; pA, polyadenylation site. **(B)** Genome replication of parental EnAd or BiTE-expressing viruses in DLD cells infected with 100 vp/cell. **(C)** Viability of DLD cells infected with EnAd or recombinant virus (MTS, five days post-infection). **(D, E)** T-cell activation (D, $CD25^+$) and target cell cytotoxicity (E, LDH release) in

co-cultures of T-cells, target cells and infected HEK293A supernatants 24 hpi. **(F)** Viability of NHDF and SKOV3 (4:1) cells monitored by xCELLigence in the absence or presence of CD3-purified PBMC (5:1 effector:target). Mean (solid line) ±SD (dotted line) of biological triplicates. **(G)** T-cell activation ($CD25^+$) in virus-infected co-cultures of NHDF and SKOV3 cells. **(H)** Representative images showing co-culture of NHDF (red, stained with CellTracker Orange CMTMR), DLD cells (unstained) and T-cells (blue, stained with CellTrace Violet), followed by infection with EnAd or BiTE-armed virus. Apoptosis was visualised using CellEvent Caspase 3/7 detection reagent (green). White arrow, dead fibroblasts. Scale bar, 100 μm.

(B-G) Data show mean ± SD of biological triplicates. Significance assessed using one-way ANOVA with Tukey's Post Hoc analysis compared to 'EnAd' (B,C) or 'uninfected' (D-G); *, $p<0.05$; **, $p<0.01$; ***, $p<0.001$.

Fig. 3. EnAd-SA-FAPBiTE does not induce T-cell activation or FAP^+ cell lysis in the absence of tumour cells. (A) Cytotoxicity in T-cell and NHDF co-cultures was assessed by LDH release 72 hpi with BiTE-expressing viruses. **(B, C)** T-cell activation in co-culture with NHDF and NHBE or SKOV3 seeded at 5:1 and infected with BiTE-armed viruses. T-cells were added 2 hpi. Activation (B, $CD69^+$; C, $CD25^+$) was assessed 72 hpi. **(D)** LDH release in co-cultures from (B, C). **(E)** T-cell activation ($CD25^+$) and **(F)** LDH release in co-cultures of fresh bone marrow samples five days post-infection with FAP-BiTE-expressing EnAd. Prior to virus infection, bone marrow cells were plated with NHDF with or without SKOV3 (50:5:1). LDH release was calibrated against lysis of corresponding amounts of NHDF and SKOV cells without bone marrow cells, corrected for the amount released by healthy bone marrow cells.

822

823 Data show mean ± SD of biological triplicates. Significance between more than two conditions
824 was assessed using one-way ANOVA with Tukey's Post Hoc analysis compared to
825 'uninfected' (A). Significance between two conditions was assessed using an unpaired two-
826 tailed t-test (B-F); *, $p<0.05$; **, $p<0.01$; ***, $p<0.001$.

827

828 **Fig. 4. EnAd-expressing FAP-BiTE activates endogenous T-cells and induces FAP$^+$ cell**
829 **lysis in malignant exudate samples. (A, B)** Activation (CD69/CD25$^+$) of PBMC-derived T-
830 cells co-cultured with anti-CD3/CD28 Dynabeads (A) or NHDF and BiTEs (B) for 24 hours in
831 normal serum or ascites fluid (50%). **(C)** Representative flow cytometry plot demonstrating
832 the cellular composition for a typical ascites biopsy sample. **(D)** PD-1 expression by T-cells as
833 a percentage of total CD3$^+$ cells. **(E)** CD25 expression on endogenous T-cells five days post-
834 treatment with free BiTEs or BiTE-expressing EnAd. Total unpurified cells were treated in
835 50% exudate fluid from the same biopsy sample. **(F, G)** Relative quantity of CD3$^+$ cells (F)
836 and residual FAP$^+$ cells (G). Effector:target ratios were 79.4 (sample 1, black), 2.27 (sample 2,
837 blue), 31.6 (sample 3, red) and 2.44 (sample 4, grey). **(H)** Cytokine production was evaluated
838 by a multiple human Th cytokine panel. **(I)** TGFβ in supernatants harvested from ascites cells
839 incubated with PBMC T-cells and BiTE-expressing virus.

840

841 (A,B,E-I) Data show mean ± SD of biological triplicates. Significance was assessed using one-
842 way ANOVA with Tukey's Post Hoc analysis compared to 'normal serum' (A,B) or 'untreated'
843 (E-I). (D) Data show mean ± SD. Significance assessed using an unpaired two-tailed t-test; *,
844 $p<0.05$; **, $p<0.01$; ***, $p<0.001$.

Fig. 5. Global response of malignant ascites to infection with EnAd-SA-FAPBiTE. (A) Heat map showing changes in mRNA counts (as global significance score, average of three samples) within defined gene-sets compared to untreated. Left, EnAd-SA-controlBiTE; right, EnAd-CMV-FAPBiTE. **(B)** Fold-change plot showing gene-specific differences in mRNA counts following infection of biopsy 4 with EnAd-SA-FAPBiTE. Five T-cell activation (blue) and fibroblast (gold) markers are shown. COL3A1, alpha1 (III) collagen; THY1, Thy-1; IL13RA2, IL-13Rα2; FN1, fibronectin; GZMB, granzyme B; PRF1, perforin; IL2RA, CD25; IFNG, IFNγ. **(C-E)** Fold-change in mRNA counts (left, EnAd-SA-controlBiTE; right, EnAd-SA-FAPBiTE; compared to untreated) in three ascites samples for fibroblast-specific genes (C) or genes involved in T-cell function (D) or antigen presentation and T-cell trafficking (E). Circle, biopsy 4; triangle, 5; square, 6. **(F, G)** Expression levels of CD163, CD206 (F), CD64 and CD86 (G) on $CD11b^{+}CD64^{+}$ cells. gMFI, geometric mean fluorescence intensity.

(C-E) Data show mean of biological duplicates. Significant changes were assessed using a multivariate linear regression algorithm with three patient biopsies. Significance of changes in gene expression induced by each virus versus uninfected is displayed adjacent the x-axis, and between EnAd-SA-controlBiTE or EnAd-SA-FAPBiTE displayed above the plot; (F,G) Data show mean ± SD of biological triplicates. Significance was assessed using one-way ANOVA with Tukey's Post Hoc analysis compared to 'untreated'; *, $p<0.05$; **, $p<0.01$; ***, $p<0.001$.

Fig. 6. EnAd expressing FAP-BiTE activates tumour-infiltrating T-cells and mediates cytotoxicity in malignant prostate slices cultures. (A) FAP expression patterns in benign and

malignant prostate tissue slices. **(B)** Expression of viral hexon protein in prostate tissue slice following EnAd infection. **(C)** Representative image showing tumour-infiltrating T-cell activation (CD25+) in prostate tissue slices seven days post-infection. **(D, E)** IFNγ (D) and IL-2 (E) levels in malignant prostate tissue slices infected with BiTE-expressing EnAd. **(F)** Active caspase 3/7 (CellEvent Caspase 3/7 Green Detection Reagent, green) in malignant prostate tissue infected with EnAd-SA-FAPBiTE-RFP (red). White arrows, dual-positive cells; scale bar, 100 μm. **(G)** LDH release of malignant prostate tissue slices from five patients infected with recombinant EnAd. **(H)** Histological architecture and T-cell activation (CD25+) in EnAd-infected prostate slices.

(D,E,G) Data show mean ± SD of technical triplicates. For D,E, n=7; for G, n=5. Significance was assessed using one-way ANOVA with Tukey's Post Hoc analysis compared to 'uninfected'; *, $p<0.05$; **, $p<0.01$; ***, $p<0.001$.

Fig. 1

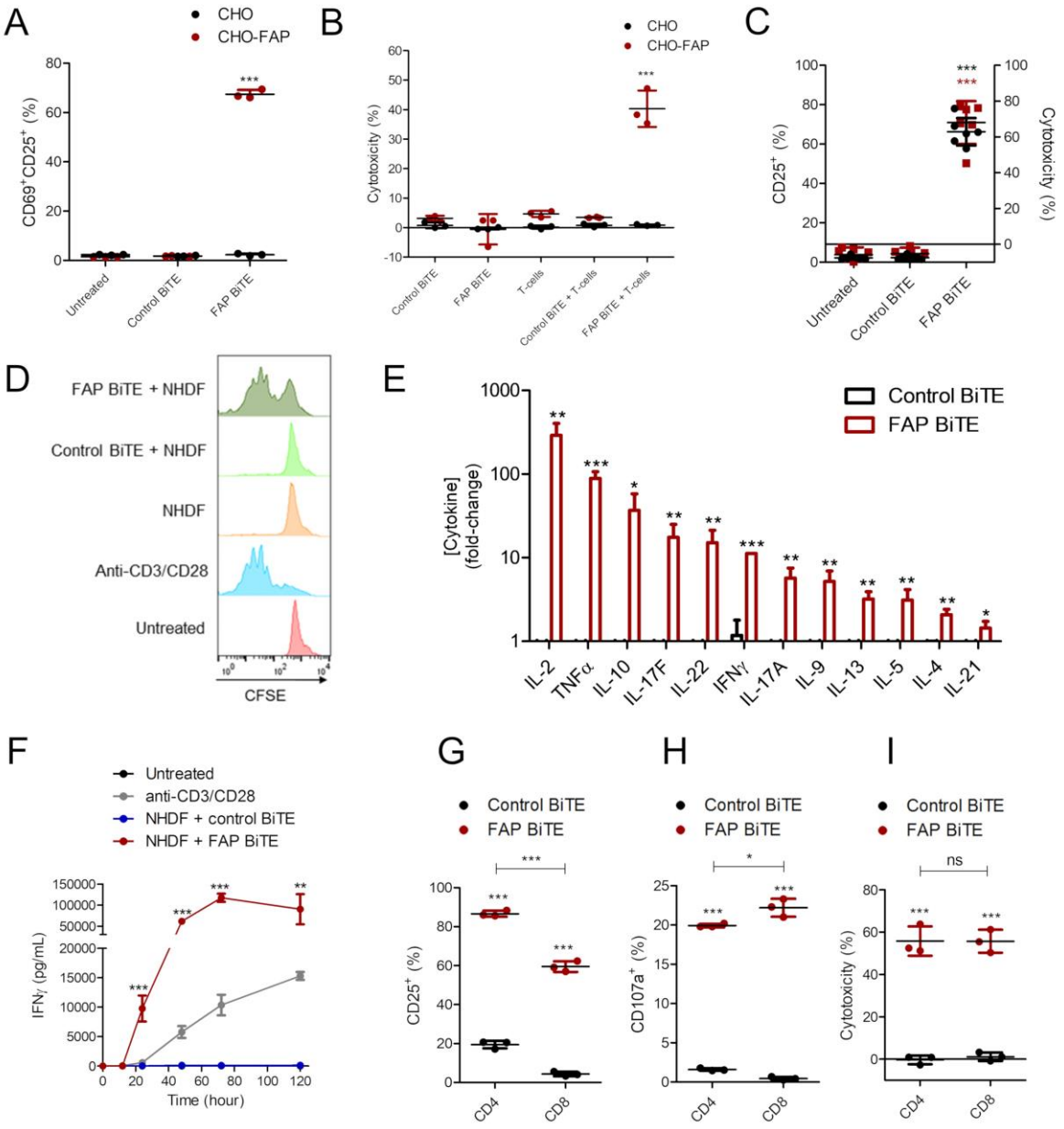
A
CHO
CHO-FAP
CD69+CD25+ (%)
Untreated
Control BiTE
FAP BiTE
B
CHO
CHO-FAP
Cytotoxicity (%)
Control BiTE
FAP BiTE
T-cells
Control BiTE + T-cells
FAP BiTE + T-cells
C
CD25+ (%)
Cytotoxicity (%)
Untreated
Control BiTE
FAP BiTE
D
FAP BiTE + NHDF
Control BiTE + NHDF
NHDF
Anti-CD3/CD28
Untreated
CFSE
E
Control BiTE
FAP BiTE
[Cytokine] (fold-change)
IL-2
TNFα
IL-10
IL-17F
IL-22
IFNγ
IL-17A
IL-9
IL-13
IL-5
IL-4
IL-21
F
Untreated
anti-CD3/CD28
NHDF + control BiTE
NHDF + FAP BiTE
IFNγ (pg/mL)
Time (hour)
G
Control BiTE
FAP BiTE
CD25+ (%)
CD4
CD8
H
Control BiTE
FAP BiTE
CD107a+ (%)
CD4
CD8
I
Control BiTE
FAP BiTE
ns
Cytotoxicity (%)
CD4
CD8

881

Fig. 2

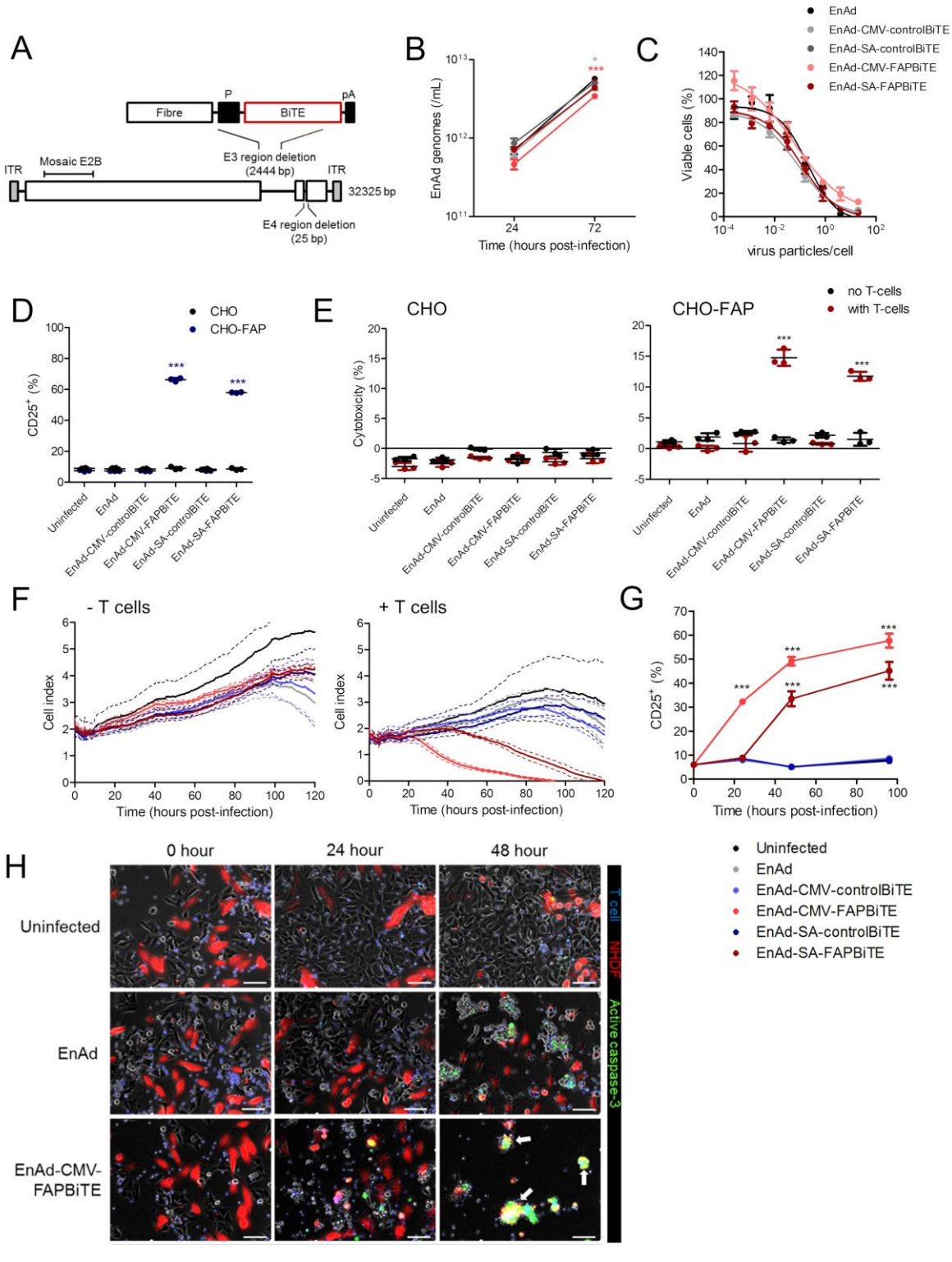
A
Fibre
P
BiTE
pA
E3 region deletion
(2444 bp)
ITR
Mosaic E2B
ITR
32325 bp
E4 region deletion
(25 bp)
B
EnAd genomes (/mL)
Time (hours post-infection)
C
Viable cells (%)
virus particles/cell
EnAd
EnAd-CMV-controlBiTE
EnAd-SA-controlBiTE
EnAd-CMV-FAPBiTE
EnAd-SA-FAPBiTE
D
CHO
CHO-FAP
CD25+ (%)
Uninfected
EnAd
EnAd-CMV-controlBiTE
EnAd-CMV-FAPBiTE
EnAd-SA-controlBiTE
EnAd-SA-FAPBiTE
E
CHO
CHO-FAP
no T-cells
with T-cells
Cytotoxicity (%)
F
- T cells
+ T cells
Cell index
Time (hours post-infection)
G
CD25+ (%)
Time (hours post-infection)
H
0 hour
24 hour
48 hour
Uninfected
EnAd
EnAd-CMV-FAPBiTE
T cell
NHDF
Active caspase 3
Uninfected
EnAd
EnAd-CMV-controlBiTE
EnAd-CMV-FAPBiTE
EnAd-SA-controlBiTE
EnAd-SA-FAPBiTE

882

Fig. 3

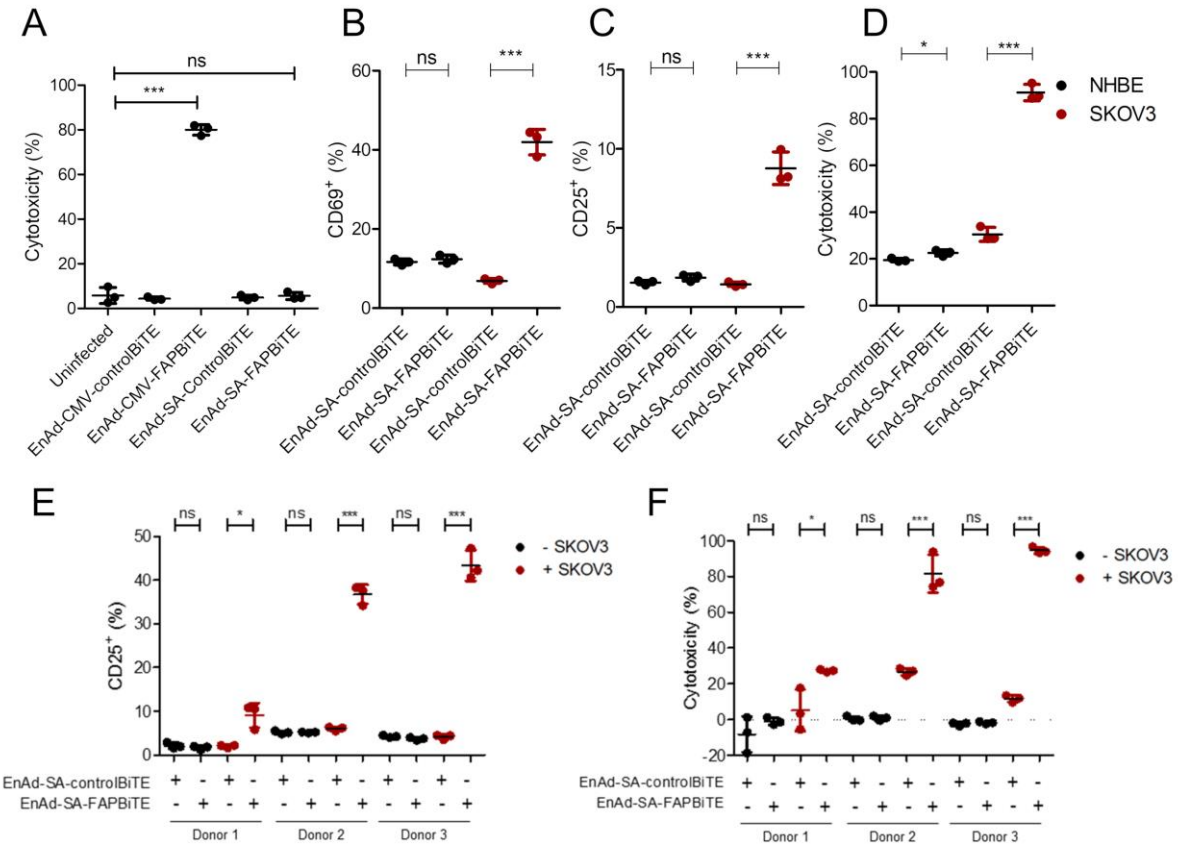
A
B
C
D
E
F
Cytotoxicity (%)
CD69+ (%)
CD25+ (%)
ns
***
*
Uninfected
EnAd-CMV-controlBiTE
EnAd-CMV-FAPBiTE
EnAd-SA-ControlBiTE
EnAd-SA-FAPBiTE
EnAd-SA-controlBiTE
EnAd-SA-FAPBiTE
NHBE
SKOV3
- SKOV3
+ SKOV3
Donor 1
Donor 2
Donor 3

Fig. 4

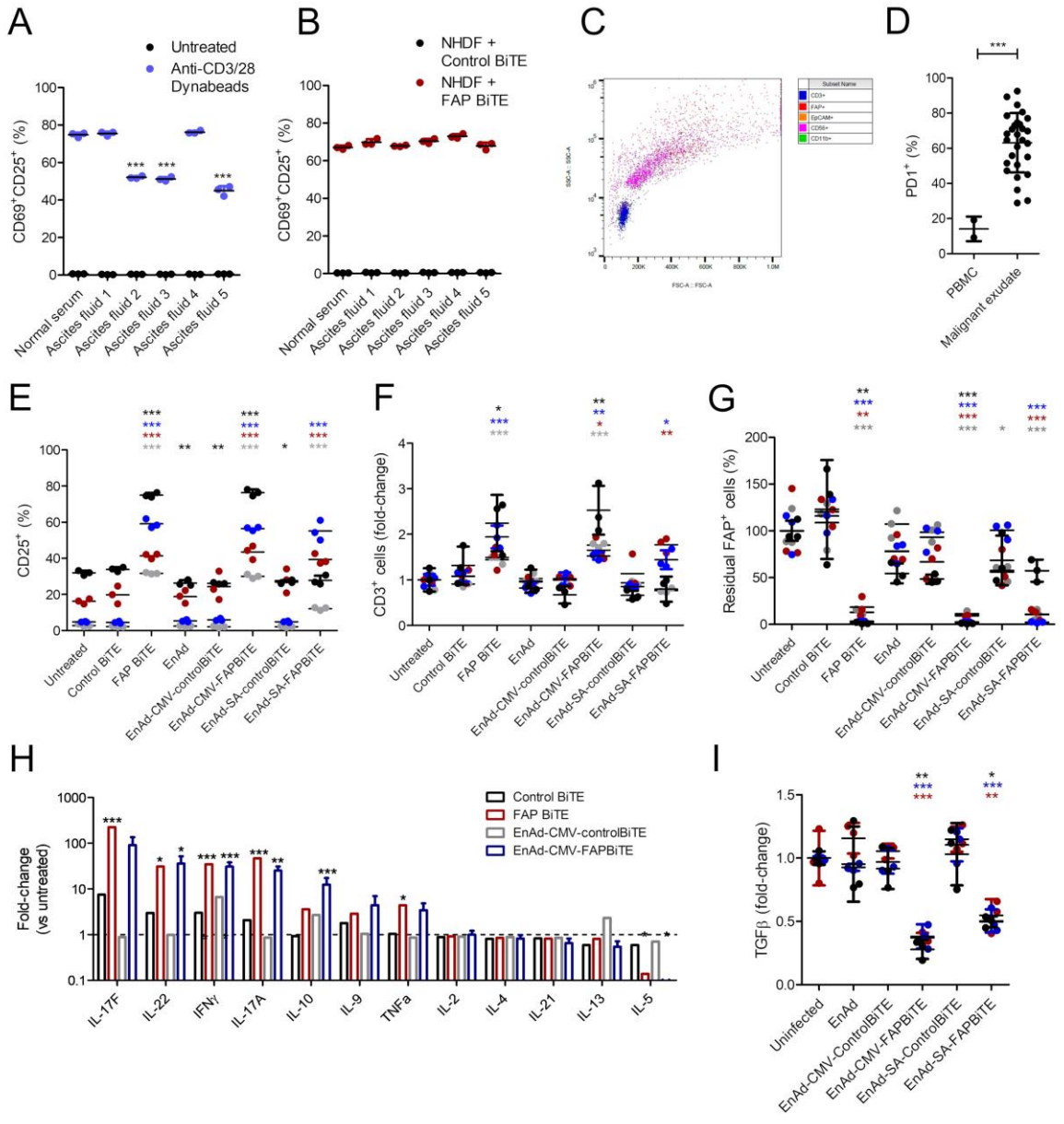
A
Untreated
Anti-CD3/28 Dynabeads
CD69+CD25+ (%)
Normal serum
Ascites fluid 1
Ascites fluid 2
Ascites fluid 3
Ascites fluid 4
Ascites fluid 5
B
NHDF + Control BiTE
NHDF + FAP BiTE
CD69+CD25+ (%)
C
D
PD1+ (%)
PBMC
Malignant exudate
E
CD25+ (%)
Untreated
Control BiTE
FAP BiTE
EnAd
EnAd-CMV-controlBiTE
EnAd-CMV-FAPBiTE
EnAd-SA-controlBiTE
EnAd-SA-FAPBiTE
F
CD3+ cells (fold-change)
G
Residual FAP+ cells (%)
H
Fold-change (vs untreated)
Control BiTE
FAP BiTE
EnAd-CMV-controlBiTE
EnAd-CMV-FAPBiTE
IL-17F
IL-22
IFNγ
IL-17A
IL-10
IL-9
TNFa
IL-2
IL-4
IL-21
IL-13
IL-5
I
TGFβ (fold-change)
Uninfected
EnAd
EnAd-CMV-ControlBiTE
EnAd-CMV-FAPBiTE
EnAd-SA-ControlBiTE
EnAd-SA-FAPBiTE

884

Fig. 5

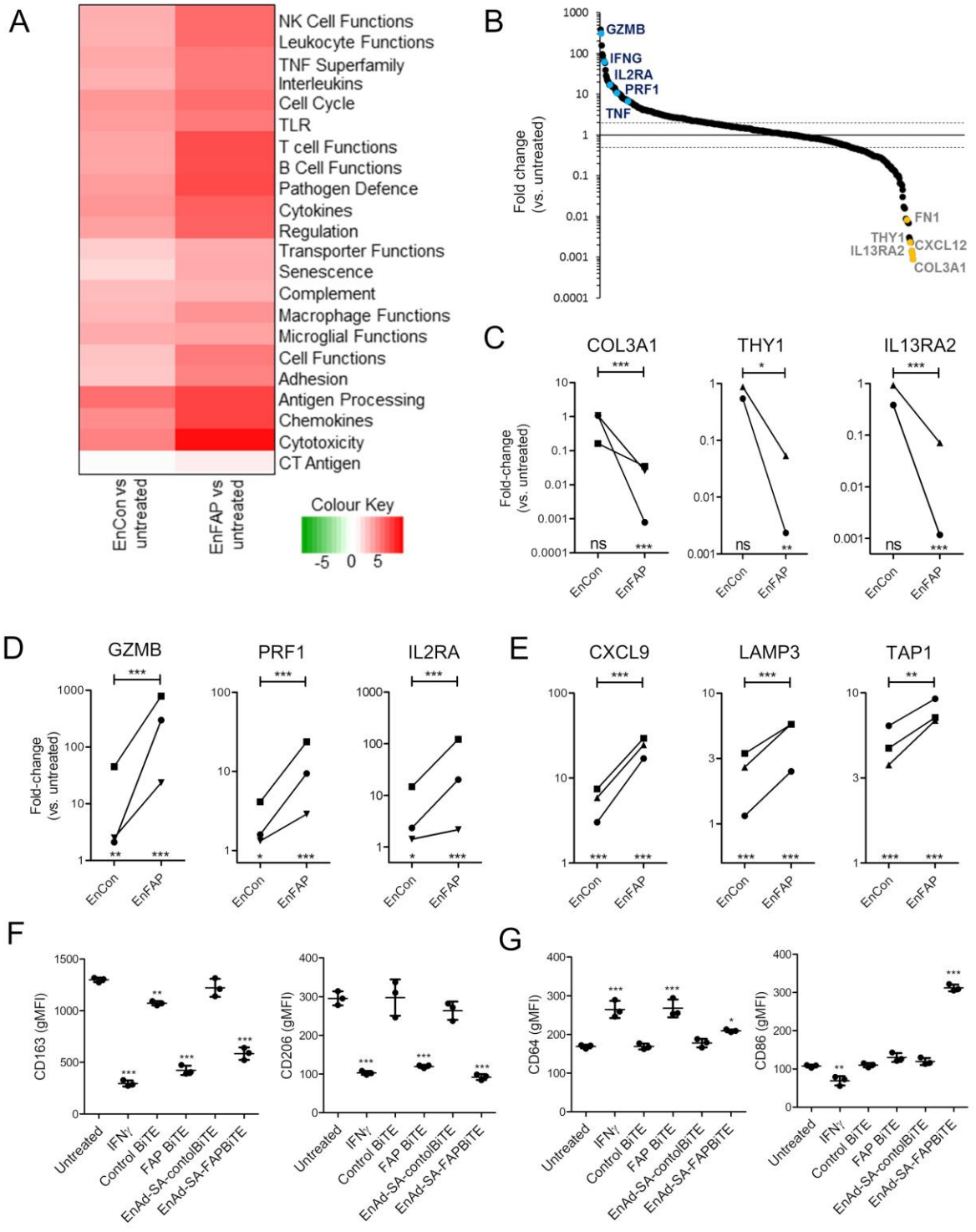
A
NK Cell Functions
Leukocyte Functions
TNF Superfamily
Interleukins
Cell Cycle
TLR
T cell Functions
B Cell Functions
Pathogen Defence
Cytokines
Regulation
Transporter Functions
Senescence
Complement
Macrophage Functions
Microglial Functions
Cell Functions
Adhesion
Antigen Processing
Chemokines
Cytotoxicity
CT Antigen
EnCon vs untreated
EnFAP vs untreated
Colour Key
-5 0 5
B
GZMB
IFNG
IL2RA
PRF1
TNF
FN1
THY1
IL13RA2
CXCL12
COL3A1
Fold change (vs. untreated)
C
COL3A1
THY1
IL13RA2
Fold-change (vs. untreated)
ns
EnCon
EnFAP
D
GZMB
PRF1
IL2RA
E
CXCL9
LAMP3
TAP1
F
CD163 (gMFI)
CD206 (gMFI)
G
CD64 (gMFI)
CD86 (gMFI)
Untreated
IFNγ
Control BiTE
FAP BiTE
EnAd-SA-contolBiTE
EnAd-SA-FAPBiTE

885

Fig. 6

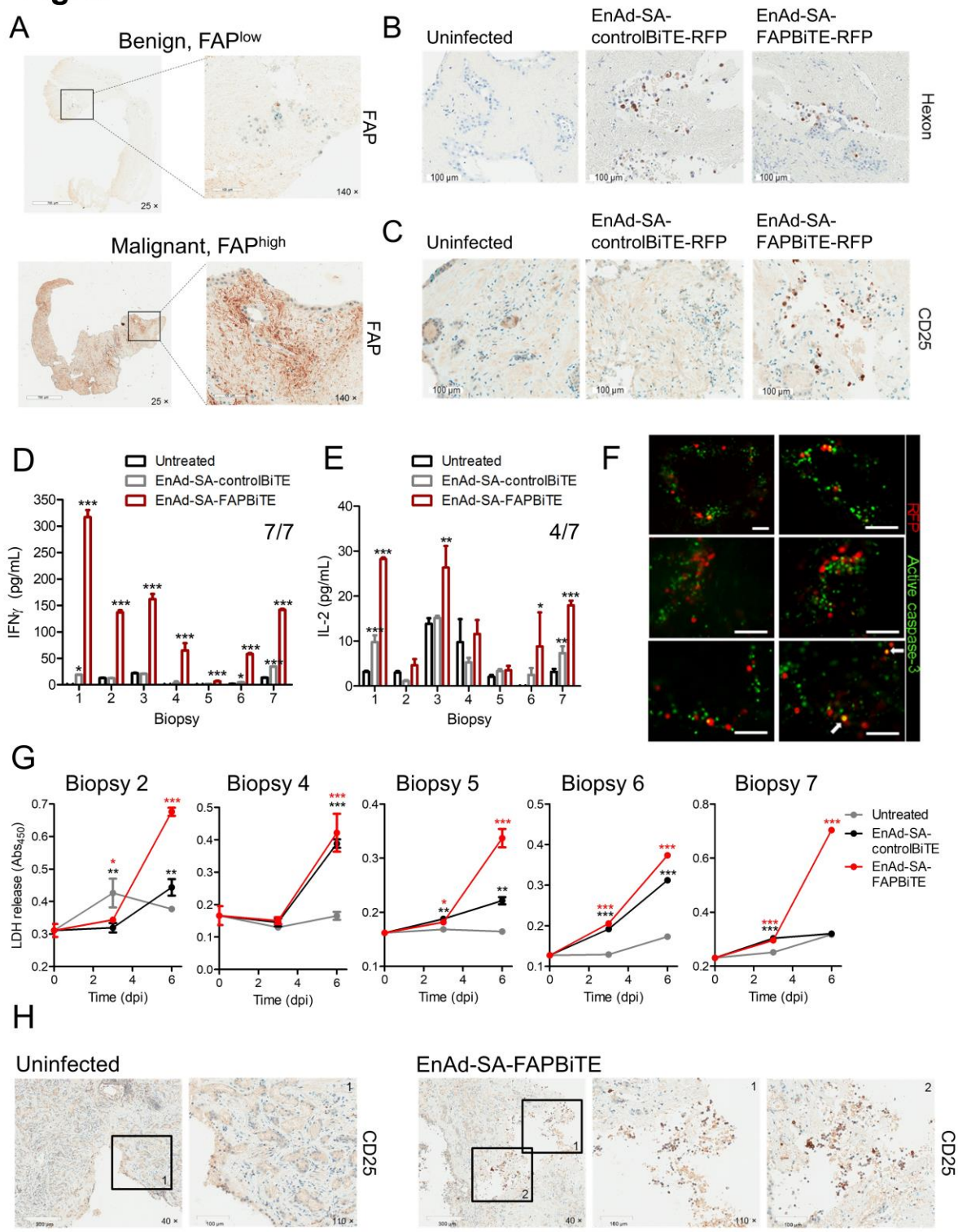
A
Benign, FAPlow
FAP
Malignant, FAPhigh
FAP
B
Uninfected
EnAd-SA-controlBiTE-RFP
EnAd-SA-FAPBiTE-RFP
Hexon
C
Uninfected
EnAd-SA-controlBiTE-RFP
EnAd-SA-FAPBiTE-RFP
CD25
D
Untreated
EnAd-SA-controlBiTE
EnAd-SA-FAPBiTE
7/7
IFNγ (pg/mL)
Biopsy
E
Untreated
EnAd-SA-controlBiTE
EnAd-SA-FAPBiTE
4/7
IL-2 (pg/mL)
Biopsy
F
RFP
Active caspase-3
G
Biopsy 2
Biopsy 4
Biopsy 5
Biopsy 6
Biopsy 7
LDH release (Abs450)
Time (dpi)
Untreated
EnAd-SA-controlBiTE
EnAd-SA-FAPBiTE
H
Uninfected
EnAd-SA-FAPBiTE
CD25

886